ACCEPTED MANUSCRIPT

Injection of Multiple Shattered Pellets for Disruption Mitigation in DIII-D

To cite this article before publication: Jeffrey Herfindal *et al* 2019 *Nucl. Fusion* in press https://doi.org/10.1088/1741-4326/ab3693

Injection of multiple shattered pellets for disruption mitigation in DIII-D

J. L. Herfindal[1], D. Shiraki[1], L. R. Baylor[1], N. W. Eidietis[2], E. M. Hollmann[3], C. J. Lasnier[4], R. A. Moyer[3]

[1]Oak Ridge National Laboratory, Oak Ridge, Tennessee, USA
[2]General Atomics, P.O. Box 85608, San Diego, California 92186-5608, USA
[3]University of California-San Diego, La Jolla, California, USA
[4]Lawrence Livermore National Laboratory, Livermore, California, USA

E-mail: herfindaljl@ornl.gov

Abstract. Plasma shutdown experiments in DIII-D have injected multiple shattered pellets at different toroidal locations for the first time, as is planned for the ITER disruption mitigation system. Systematically varying the relative timing of the two pellets suggests that simultaneously injected pellets may influence the assimilation of each other, altering the resulting disruption characteristics compared to a single pellet injecting similar neon quantities. Thermal quench (TQ) radiation measured near the injection location is reduced with the dual pellets, contrary to TQ radiation measured away from the injection ports, which does not show a clear difference between single or dual pellet injections. The mitigation of other disruption loads, such as the current quench duration and divertor heat loads, decrease when the pellets enter the plasma simultaneously compared to single shattered pellet injections with similar neon quantities. This similar reduction in mitigation of current quench and conductive loads is consistent with the observed reduction in total TQ radiation. The time between initial pellet injection and the end of the TQ is shorter when both pellets are injected simultaneously compared to a single pellet. This lower cooling duration may limit the amount of the neon assimilated by the plasma prior to the end of the TQ, consistent with the observed reduction in radiation. The injected impurities spread primarily in the parallel direction, away from the source at the injection location. The addition of two shattered pellet injectors shows that the initial poloidal radiation is spread out into two distinct regions, cooling multiple flux tubes simultaneously, which may induce global MHD instabilities more rapidly than a single flux tube of impurities leading to a shorter cooling duration. The electron density increased by approximately a factor of two with the addition of multiple pellets, but is highly sensitive to the time between injections. A maximum density increase is found when both pellets arrive at the plasma prior to the start of the TQ.

Keywords: tokamak, disruption mitigation, shattered pellet injection, multiple shattered pellet injection

Submitted to: *Nucl. Fusion*

1. Introduction

Future burning plasma devices, such as ITER, will have stored plasma energies that are considerably higher than in current devices. An unmitigated loss of plasma confinement can have enough energy release to inflict major damage upon plasma-facing components through electromagnetic loads or local deposition of thermal energy [1]. Proper mitigation of disruptions in these devices is required as a final line of defense to ensure the longevity of the first wall and plasma-facing components.

Shattered Pellet Injection (SPI) has been shown to be an effective method to mitigate disruptive loads on DIII-D [2, 3, 4]. SPI delivers high-Z impurities as a frozen pellet, which is shattered just prior to reaching the plasma to increase the surface area for efficient ablation, impurity assimilation, and avoid any possible damage to the center post from an intact pellet. Current empirical extrapolations from disruption mitigation experiments to ITER-relevant energies predict that on the order of 10^{24} neon atoms (order of magnitude more for low-Z injection such as deuterium) are needed to adequately mitigate thermal loads and electromagnetic forces [5, 6]. Practically reaching these quantities of impurities requires the use of multiple SPI systems injecting pellets simultaneously into the plasma. The use of multiple SPI systems has some beneficial effects, such as increased system redundancy, but also raises some questions regarding the acceptable scatter in arrival time between pellets. The arrival of the first pellet marks the start of the disruption mitigation process and the effectiveness of the remaining pellets may be reduced by entering a colder plasma than expected. This can result in a lower mixing efficiency and plasma-cooling impurity radiation which may lead to excessive conductive heat loads to the divertor. This paper presents the first results of dual SPI mitigation and compares each measured parameter to a similar SPI injection with low or high Ne quantities.

This paper is organized as follows: Section 2 describes the experimental method, typical plasma and pellet parameters, and determination of the pellet arrival time. Section 3 presents the common measurable disruption mitigation parameters. Section 4 shows measurements of the initial radiation from SPI following helical flux tubes. Section 5 discusses the implications of these results for future SPI disruption mitigation systems. Section 6 summarizes the main conclusions.

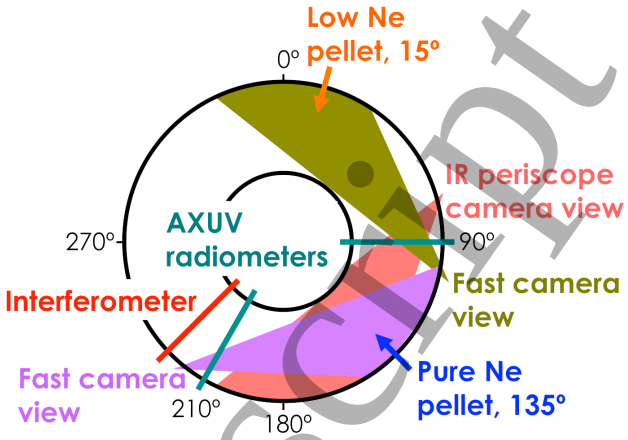

Figure 1. Top-down schematic of pellet injection and diagnostic locations.

2. Experimental Method

This experiment examined the change in common disruption mitigation properties (such as radiation fraction, radiation asymmetries, peak divertor and wall heat flux, and current quench duration) through two SPIs either simultaneously or with a slight time delay between injections. The quantity of the primary radiator, Ne, within the two pellets is chosen to have a measurable difference in radiation fractions and current quench (CQ) duration if they were injected individually. Previous work has shown that increasing the neon quantity within a pellet increases radiation fractions during the thermal quench (TQ) and first wall heating as well as decreasing CQ duration, peak halo current loads, and inner strike point thermal loads [4]. The two pellets consisted of a mixed species pellet containing 1.3 Pa-m^3 of neon (3.2×10^{20} atoms) and 36 Pa-m^3 of deuterium (1.8×10^{22} atoms) and a pure 53 Pa-m^3 neon pellet (1.3×10^{22} atoms). Hereafter, the mixed species pellet is referred to as the low Ne pellet. The timing between injections is systematically varied in order to establish a baseline radiation fraction when each pellet mitigates the plasma individually as well as when they both enter the plasma prior to the dissipation of the stored thermal energy at the end of the TQ.

SPI locations and diagnostics used to measure

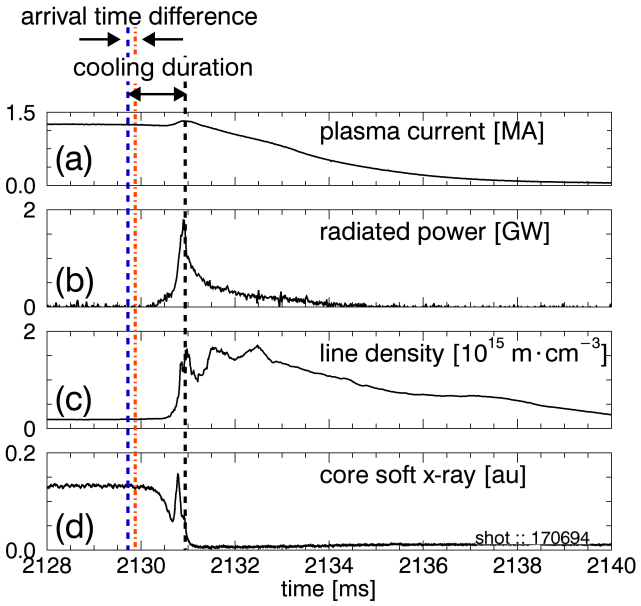

Figure 2. Example of a mitigated discharge using multiple pellets showing the plasma current (a), radiated power (b), line-integrated density (c), and a core soft x-ray channel (d). The pure neon pellet arrived first, illustrated by the blue dashed line, starting the mitigation process. The low Ne pellet arrived later (orange dash-dot line) prior to the end of the TQ (black dashed line).

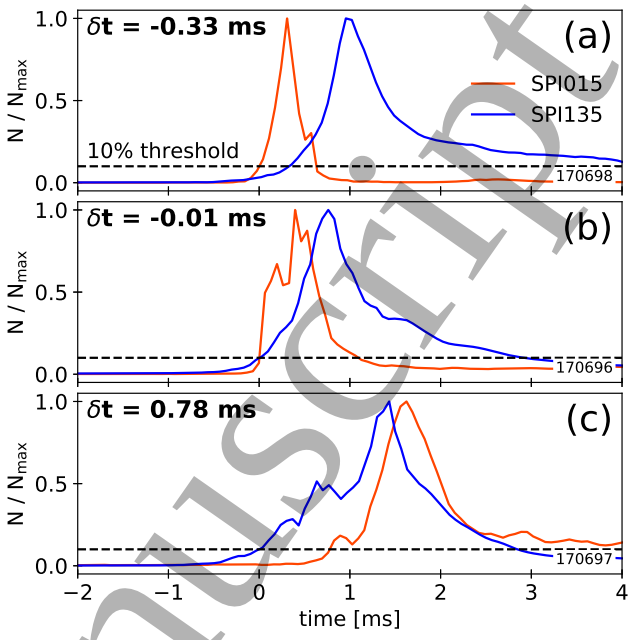

Figure 3. Normalized signal from the two visible fast-framing cameras, integrated within a boxed region surrounding the initial pellet trajectory. Examples are shown of the low Ne pellet arriving first (a), both pellet arriving at the same time (b), and the pure Ne pellet arriving first (c).

disruption mitigation properties are shown in Fig. 1. The low Ne pellet is injected at 15 degrees toroidally from SPI015 [7] and the pure Ne pellet is fired from the injector [8] located at 135 degrees (SPI135). Each pellet is injected from a similar poloidal location, $\sim$45 degrees above the mid-plane. The radiated power is measured using x-ray/ultra-violet (AXUV) diode arrays at 90 degrees [9] and the DISRAD-II system at 210 degrees [10]. Both of these systems are a pinhole-type camera with no filter in order to measure the total radiated power. Two fast-framing visible cameras are used to determine the arrival of each pellet and are discussed further in Section 2.1. Conducted heat loads in the divertor as well as radiated heat loads on the first wall are measured using an infrared periscope [11] near the pure Ne pellet injection location. Line-integrated electron density is measured with a CO_2 interferometer observing the plasma radially across the mid-plane at 225 degrees [12].

The same target lower single-null neutral beam heated H-mode plasma is used for each discharge presented in this paper. Typical plasma parameters consist of a plasma current, I_p, of 1.3 MA, toroidal magnetic field, B_T, of 1.67 T, normalized plasma beta of 1.9, line-integrated density of 7.5×10^{14} m $\cdot$ cm^{-3}, and a safety factor at the 95% flux surface, q_{95}, of 3.2. A typical mitigated discharge using multiple pellets shown in Fig. 2 illustrates the plasma current (a), radiated power (b), line density (c), and a core soft x-ray channel (d). This discharge shows the pure neon pellet starting the mitigation process arriving first (blue dashed line) followed by the arrival of the low Ne pellet (orange dash-dot line). The arrival time difference, used for the x-axis in Figs. 4 - 7(a), is defined as the arrival time of the pure Ne pellet subtracted from the arrival time of the low Ne pellet. The cooling duration is the time between the arrival of the first pellet and the end of the TQ (black dashed line). It is important that the second pellet arrives within the cooling duration time window (on the order of 1 ms for this plasma) in order for both pellets to contribute to the TQ mitigation.

2.1. Determination of pellet arrival time

The pellet arrival time is ascertained using two visible fast-framing cameras [13] observing each SPI port through a Ne I filter at 640.2 nm. The counts from the camera are integrated over time within a square box region encompassing the injection port and plasma edge, encompassing the shattered pellet plume trajectory. The pellet arrival time is found when the integration of the counts (N) within the boxed region reached 10% of the maximum number counts (N_{max}) observed within the region. Error bars for the arrival time are defined as the time required for the integrated counts to go from 10% to 20% of

the peak value. It is found that the individual SPI arrival times would vary slightly (up to ∼0.5 ms for some cases) based on the box location. However, if similar regions were chosen for SPI015 and SPI135 (e.g. at the separatrix or encompassing the injection port) the difference in arrival times would offset each other and the overall picture of the results presented in Section 3 do not change significantly enough to change the interpretation.

Examples of different pellet arrival times is shown in Fig. 3 for three different discharges: (a) the low Ne pellet arrived first by 0.33 ms, (b) when the pellets arrived simultaneously, and (c) when the pure Ne pellet arrived first by 0.78 ms. The dashed lined in each subfigure represents the 10% threshold where the pellet arrival time is defined. The x-axis for each case is offset in time in order for the arrival of the first pellet to be at 0 ms.

3. Dual SPI characteristics

This section covers measurable disruption mitigation parameters such as radiation, first wall and inner strike point heat loads, and CQ duration. Each subsection explains how each measurement is performed and the analysis techniques used.

3.1. Radiation near the injection ports

The radiated power is reconstructed from the inversion of AXUV diode array measurements assuming the majority of the emission is near the separatrix (the "mantle" model) [10]. The radiated power is not normalized to the absolutely calibrated foil bolometers on DIII-D because of the different toroidal location of each detector and the unknown toroidal radiation behavior during the TQ. However, all data presented in this paper is from the same run-day, allowing for dual SPI behavior to be extracted from observed trends in the data by minimizing errors introduced through photodiode degradation due to neutron damage [14]. The radiated power is scaled to match the measured power at 210 degrees through averaging the ratios of integrated power from 0.5 ms after the start of the CQ to the end of the CQ. This method assumes that the radiation is axisymmetric in this phase, which has been observed in other mitigated discharges [15]. This allows for the direct comparison of the TQ radiation at two different toroidal locations (the radiation at this second location is discussed further in Section 3.4).

Fig. 4(a) shows the radiation measured near the injection ports at 90 degrees toroidally. The measured radiation is defined as the reconstructed emissivity multiplied by the plasma volume normalized to the stored thermal energy determined through plasma reconstructions using EFIT [16] prior to the disruption. This does not account for TQ radiation asymmetries which may exist in the TQ radiation. The x-axis is the arrival time difference (outlined in Fig. 2). Points to the right of the 0 ms dividing line have the pure Ne pellet radiating and arriving at the plasma first. The blue triangles represent discharges where the low Ne pellet arrived after the TQ and did not contribute to the TQ mitigation.‡ Therefore, these discharges are treated as pure Ne SPI mitigated plasmas. The black diamonds represent discharges where both pellets arrived prior to the end of the TQ§ and the orange circles are discharges where only the low Ne pellet is injected into the plasma.‖

Previous pellet composition scans – varying the neon composition within the pellet – found global TQ radiation fractions to increase from ∼0.5 using a low Ne pellet to >0.9 using a pure neon pellet [4]. The left and right extremes of Fig. 4(a) are in agreement with previous measured radiation fraction trends for a single low Ne quantity pellet with a low radiation fraction and a pure Ne pellet exhibiting higher radiation fractions. However, the TQ radiation fraction is reduced when both of the pellets enter the plasma simultaneously (an arrival time difference of 0 ms) despite having a combined neon impurity quantity higher than the pure neon pellet alone. The radiation fraction during simultaneous injection should be comparable to the single pure Ne pellet, suggesting that the addition of the second pellet impacts the assimilation of the other pellet. This result is discussed further in Section 5.

3.2. Peak heat flux measurments

An infrared periscope [11] is used to measure conducted and radiated divertor and wall heat loads observing near the pure Ne pellet injection location (see Fig. 1). Extrapolation of post-disruption temperature decay allows for the determination of heat loads emitted from the plasma during the TQ [17]. Fig. 4(b) shows the heat load incident on the inner strike point (divertor) and Fig. 4(c) is the heat load to a location on the first wall (right below the injection point). Comparison of the left and right extremes of Fig. 4(c) show the increased impurity content of the pure Ne pellet results in more radiation leading to a higher heat flux to the first wall. Similarly, the increase in radiation because of the pure Ne pellet decreases the heat load incident on the inner strike point. Intermediate cases show a decrease in heat load observed on the first wall and an increase in heat load from the inner strike point compared to the pure Ne pellet extreme. This implies that there are less radiation losses in the plasma due to

‡ SPI135 shots: 170701 and 170707
§ Dual SPI shots: 170693, 170694, 170695, 170696, 170697, 170698, 170700, 170703, 170705, and 170709
‖ SPI015 shots: 170702 and 170706

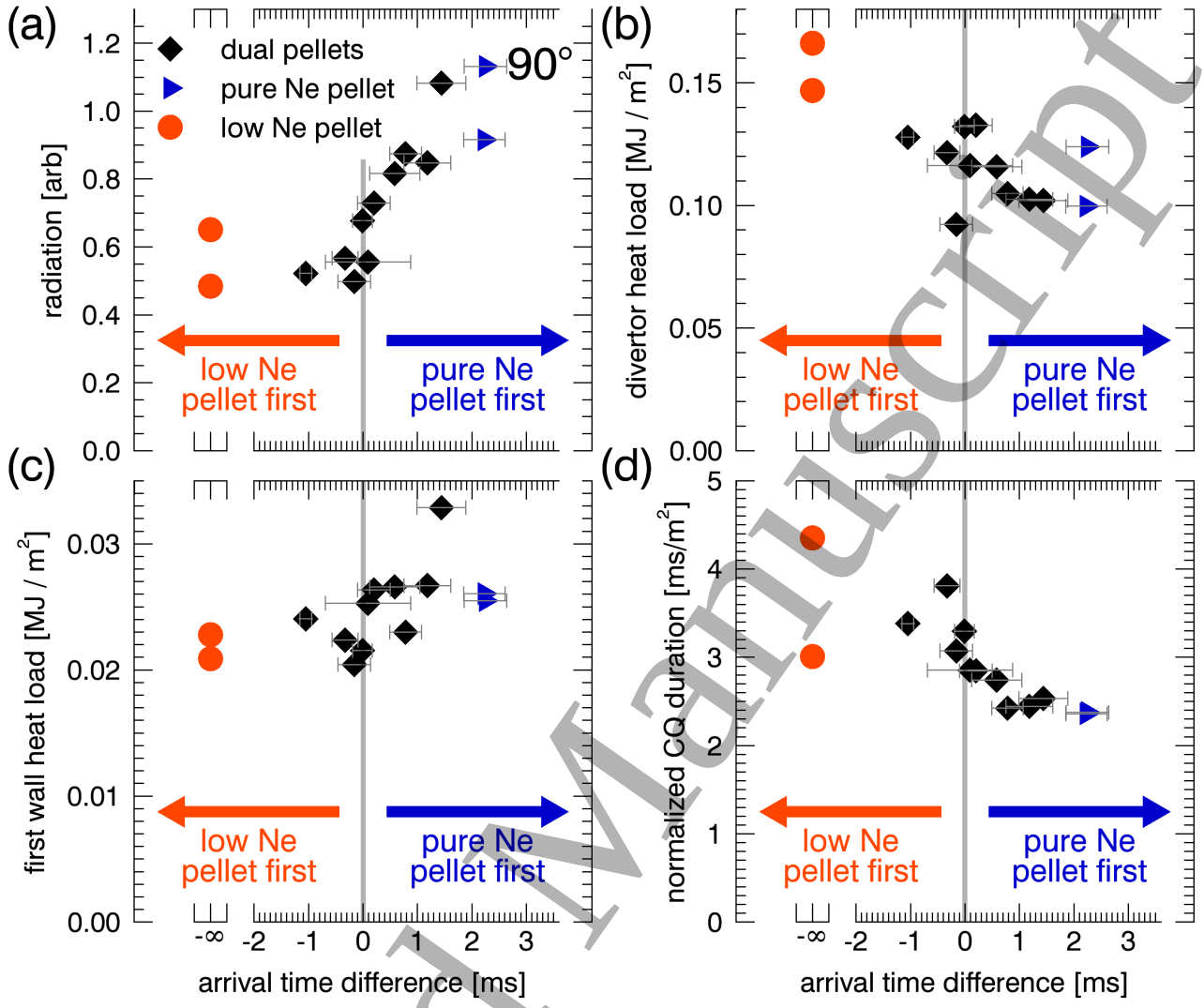

Figure 4. Radiation near the injection port (a) decreases as pellets enter the plasma simultaneously (black diamonds) compared to when a pure Ne pellet is the sole contributor to the TQ mitigation (blue triangles). Simultaneous pellet injection still has better mitigation than when the low neon quantity pellet mitigates the plasma (orange circles). Peak heat flux extrapolations using a IR periscope measurements near the pure Ne pellet injection port show a decrease in peak heat flux incident on the inner strike point for the pure Ne pellet cases (b). This decrease in peak heat flux is accompanied by an increase in peak heat flux upon the first wall (c). The intermediate cases, near an arrival time difference of 0 ms, show an increased inner strike point (b) and a decrease in first wall (c) heat flux compared to when pure Ne pellet is the sole contributor to the TQ. Similarly, the CQ duration (d) increased for intermediate cases indicating a reduction in global radiation.

the injection of both pellets, confirming the observed trend in the radiation fraction near the injection ports.

3.3. Current Quench duration

The current quench (CQ) is the result of an increase in plasma resistivity following the TQ [18]. The plasma resistivity following the TQ is closely tied to the electron temperature following the TQ. Experiments on DIII-D have shown that an increase in radiated power (due to a higher primary radiator concentration within a SPI) leads to a more resistive plasma with a shorter normalized CQ duration [4]. Consequently, the CQ duration provides information relating the global plasma resistivity after the TQ compared to more localized radiation measurements presented in Section 3.1 and Section 3.2.

The CQ duration shown in Fig. 4(d) is found through a linear fit of the plasma current from the peak value at the end of the cooling duration to 80% of the peak value. The normalized CQ duration reported is the interpolation of this linear fit from 100% to 0% divided by the poloidal cross-sectional area prior the TQ.

Comparison of the extremes of Fig. 4(d) show a shorter CQ duration for the pure Ne pellet cases

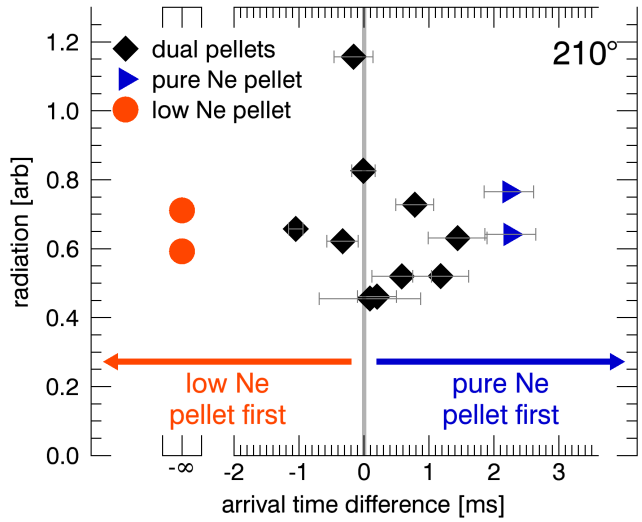

Figure 5. Radiation away from the injection locations do not have a clear difference between low Ne pellet injection (orange circles) and the pure Ne pellet injections (blue triangles).

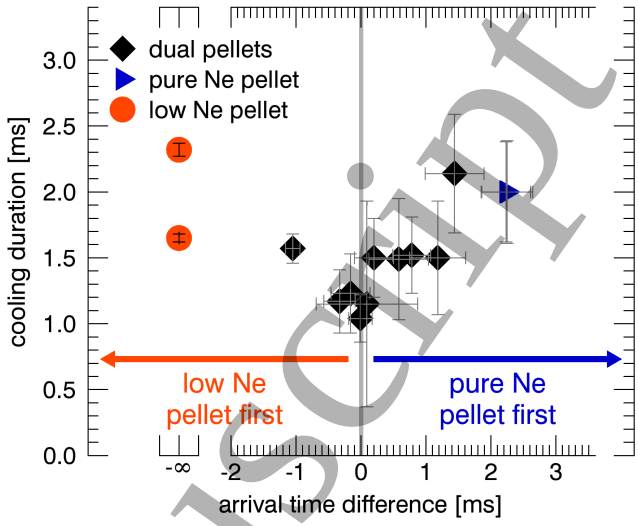

Figure 6. Measured cooling duration (the time between when the first pellet enters the plasma and the end of the TQ; see Fig. 2) is reduced when multiple pellets enter the plasma simultaneously.

compared to the low Ne pellet mitigated plasmas. The CQ duration increases as the time between pellet arrivals approaches zero for the dual pellet discharges compared to the plasmas mitigated by the pure Ne pellet. This suggests that less energy is radiated away leading to a lower resistivity and a longer current quench. This is consistent with the measurements presented in Sections 3.1 and 3.2.

3.4. Radiation behavior away from injection location

Fig. 5 shows the radiation fraction measured away from the injection ports at 210 degrees. The trend in the radiation fraction at this location is completely different than the radiation fraction near the injection port shown in Fig. 4(a). First, the left and right extremes of the plot do not show an increase in radiation fraction for a pure Ne pellet compared to the low Ne pellet. Second, the overall trend within intermediate cases is flat, showing no decrease or increase.

The similar radiation fraction observed at this toroidal location between the pure and low Ne pellets gives information about possible radiation asymmetries and preferential flow direction of the injected impurities. More insight is gained when the measurements in Fig. 5 are combined with the results from a previous pellet composition scan which used a similar plasma target [4]. The previous pellet composition scan fired each pellet from SPI015 and measured the radiation at 210 degrees. They found that the pure Ne pellet produced more radiation compared to a low Ne pellet. The primary difference between this experiment and the data shown in Fig. 5 is the toroidal distance traveled by the pure Ne pellet since the toroidal distance traveled by the low Ne pellet is identical for both cases. The shortest toroidal distance which the pure Ne pellet had to travel to reach the detector at 210 degrees is 165 degrees counter-clockwise for the previous pellet composition experiment and 75 degrees clockwise for this experiment. Since a higher radiation fraction (relative to the low Ne pellet) is found in the previous pellet composition experiment, this suggest that the counter-clockwise direction is the preferred parallel flow of the injected impurities, towards the high-field side based on the helicity of the equilibrium field. The preferential high-field side radial flow is predicted for the initial spreading of Massive Gas Injection (MGI) discharges [19] but has not been observed experimentally on DIII-D [20].

Additionally, the pure Ne pellet radiation within this experiment is higher at the radiometer located in the counter-clockwise direction (90 degrees) compared to the radiometer located clockwise from the injection port (210 degrees; ~1.0 compared to ~0.7). This also indicates that there is a preferred high-field side parallel flow since the additional distance traveled to the detector in the clockwise direction is minimal. The radiation for the low Ne pellet has a similar increase for the detector located counter-clockwise (~0.65; Fig. 5) compared to the detector located clockwise from the injection [~0.55; Fig 4(a)].

3.5. Plasma cooling duration

The plasma cooling duration is defined in Fig. 2 as the time between the arrival of the first pellet and the end

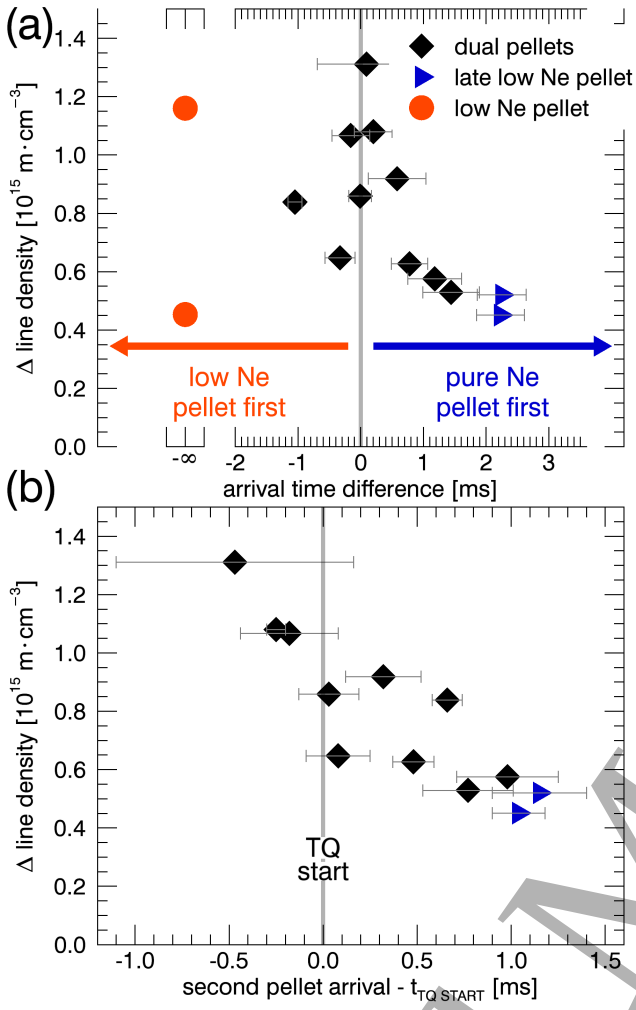

Figure 7. The increase a radial measurement of the line-integrated density (a) for the low Ne pellet cases (orange circles), dual pellet cases (black diamonds), and when the pure Ne pellet solely mitigated the TQ (blue triangles). The same increase in density shown in (a) plotted for each dual pellet case as a function of the arrival time of the second pellet minus the start of the thermal quench (b), showing that the maximum density increase is found when the second pellet arrives before the start of the CQ (simultaneous injection).

of the TQ (or start of the CQ). The cooling duration provides an upper limit on the time for the shattered pellet plume (from either pellet) to enter the plasma in order to contribute to the TQ mitigation. Fig. 6 shows the cooling duration for the dual SPI mitigations presented in this paper. The plasma cooling duration is comparable for either low or pure Ne single pellet injection but is lower when both pellets are injected simultaneously. The cooling duration is discussed further in Section 5.

3.6. Electron density

This experiment has three distinct SPI scenarios to compare the increase in electron density: the injection of a single pellet, the injection of multiple pellets prior to the end of the TQ, and the injection of multiple pellets where one pellet arrives after the TQ but before the end of the CQ. Despite the different SPI scenarios, the radial line-integrated electron density shown in Fig. 2(c) is typical for SPI mitigated shutdowns during this experiment. The density measured at the location shown in Fig. 1 increases as the impurities spread from their injection location. The density continues to rise until the start of the CQ where it then remains relatively constant until the plasma current decays to below ~50% of its peak value. The increase in density for each discharge is found by subtracting the density prior to pellet injection from the average of the density when the plasma current is between 80% to 60% of its peak value. This time frame after the injection of each pellet is chosen to be representative as the average maximum density during the start of the CQ because of its relevance to suppress the formation of a runaway electrons. It is assumed that the electron density is approximately toroidally symmetric during this time frame.

Fig. 7(a) shows this increase in the line-integrated radial electron density. The two low Ne pellet cases (orange circles) have drastically different values, with one over double the density increase of the other. Analysis of four previous SPI mitigated discharges in DIII-D using similar plasma targets and pellet compositions¶ produce a change in line density of 0.2 to 0.4 $\times 10^{15}\,\mathrm{m}\cdot\mathrm{cm}^{-3}$ (not shown in plot). The reason for the significant outlier within the low Ne pellet shots in this experiment is unknown and does not appear to be typical. The electron density increase for the pure Ne pellets is similar to the low Ne pellet cases despite having both pellets contribute to the CQ mitigation (the low Ne pellet arrived during the CQ already initiated by the pure Ne pellet, see Section 3.1). The low effectiveness of pellets to increase the density that arrive during the CQ is most likely because of the poor ablation and ionization rates of a cold plasma. The dual pellet cases (black diamonds) show an increase in density when both pellets enter the plasma simultaneously compared to the single pellet cases. The increase in density is sensitive to the timing delay between the pellets. Dual pellet cases with an arrival time difference of ~1 ms already show a decrease in density compared to the <0.5 ms cases.

The decrease in effectiveness for the second pellet to increase the density relative to its arrival time is further illustrated in Fig. 7(b). The y-axis is the same

¶ shots: 160624, 160625, 160626, and 160627

as in (a), but the x-axis is the arrival time of the second pellet subtracted from the start of the TQ (defined as when the radiated power is 10% of its peak value). The change in radial line density decreases as the arrival of the second pellet crosses the start of the TQ (solid grey line) and continues to drop to values comparable to single pellet cases as the plasma continues to cool.

4. Initial SPI radiation

The initial radiation (radiation up to 10% of the peak value) behavior at the AXUV radiometer at 90 degrees [shown in Fig. 1(a)] for three SPI cases: (1) the injection from SPI015, (2) from SPI135, and (3) the dual pellet cases discussed in Section 2. Since only the spatial localization of the initial TQ radiation is considered, shots within the cases using low or high Ne quantities of the pellets are not differentiated. It is found that the initial radiation from SPI follows the helical field lines toroidally around the plasma based on the initial injection location.

The magnetic field lines (just inside the separatrix) along the radial trajectory of the shattered pellet were calculated with TRIP3D [21] for each injection location (SPI015 and SPI135). The field lines are then followed from the initial injection location to the radiometer at 90 degrees following the minimal toroidal distance between the injected impurities and the radiometer. The location of these field lines is shown in Fig. 8 for injections originating from SPI015 (green squares) and SPI135 (purple circles). Specific radiometer chords from the upper array (teal) and lower array (orange) are highlighted if they overlap these field lines. The signal for each radiometer channel is integrated from just before the injection until the radiated power reconstruction (technique discussed in Section 3.1) reached 10% of its maximum value. The integrated signals for each discharge are subsequently added together corresponding to channel number then normalized by the number of shots to create the plots shown in Fig. 8(b) - (d).

Case one involved five shots[+] all fired from SPI015 transversing 75 degrees clockwise (see Fig. 1).* The histogram of the initial signal for this case, Fig. 8(b), shows that the majority of the signal is near channel 5 in the upper array. The lower array has a broad distribution near channel 11, primarily due to the close proximity of the field lines to the detector. The illuminated channels match the location of the field lines originating near the injection location transversing to the lower right corner shown for SPI015 in Fig. 8(a). This signifies that the majority of the ionized injected impurities initially radiate within the plasma helically along the field lines based on their injection location. Similarly, the field lines for an injection originating from SPI135 would illuminate channels near 6 in the lower array and channels near 23 in the upper array. Fig. 8(c) shows the data from the second case consisting of two discharges.‡ Both the upper and lower arrays have a sharp distribution near the location predicted by the field line trajectory, further confirming that the injected impurities initially radiate along the field lines originating at their injection location. The third case shown in Fig. 8(c) consists of eight dual SPI shots.†† The signal in the upper array shows that there are two distinct regions of radiation, each corresponding with the location of SPI135 only shots in (c) and SPI015 shots in (b). Each one of these shots consistent of pellets discussed in Section 2 where SPI015 fired a low Ne pellet and SPI135 fired a pure Ne pellet.

The injected impurities spread primarily in the parallel direction, away from the source at the injection location. This shows that the initial SPI radiation can be spread out poloidally depending on the edge safety factor and the toroidal injection location. The helical nature of cooling rational flux surfaces is also found for SPI simulations using pure deuterium pellets in JET plasmas where the pellets induced rapid cooling along field lines through parallel heat conduction [22]. Measurements of the initial radiation at 210 degrees is inconclusive, possibly due the the weak signal from the radiating impurities far away from the injection location. Initial analysis of the poloidal radiation behavior during the TQ shows each case primarily radiating from the plasma core but is left for future analysis.

5. Discussion

This experiment is the first time in which more than one shattered pellet is used to mitigate a plasma. The primary result, that the radiation fraction may not be cumulative, is rather unexpected. This raises a concern for future burning plasma devices about how much high-Z impurity is required to adequately radiate the stored thermal energy uniformly around the plasma facing components. In particular, impurity injection quantities estimated based on extrapolation of single pellet results may underestimate the required quantities for mitigation based on multiple injections in ITER.

A possible mechanism for the reduction in total assimilation is the change in disruption onset

[+] SPI015 shots: 170702, 170703, 170706, 173664, and 173672

* Note: Some shots have changed from dual SPI to SPI015 shots because the second pellet arrived after the radiated power threshold.

‡ SPI135 shots: 170708 and 170709

†† Dual SPI shots: 170693, 170694, 170695, 170696, 170697, 170698, 170700, and 170705

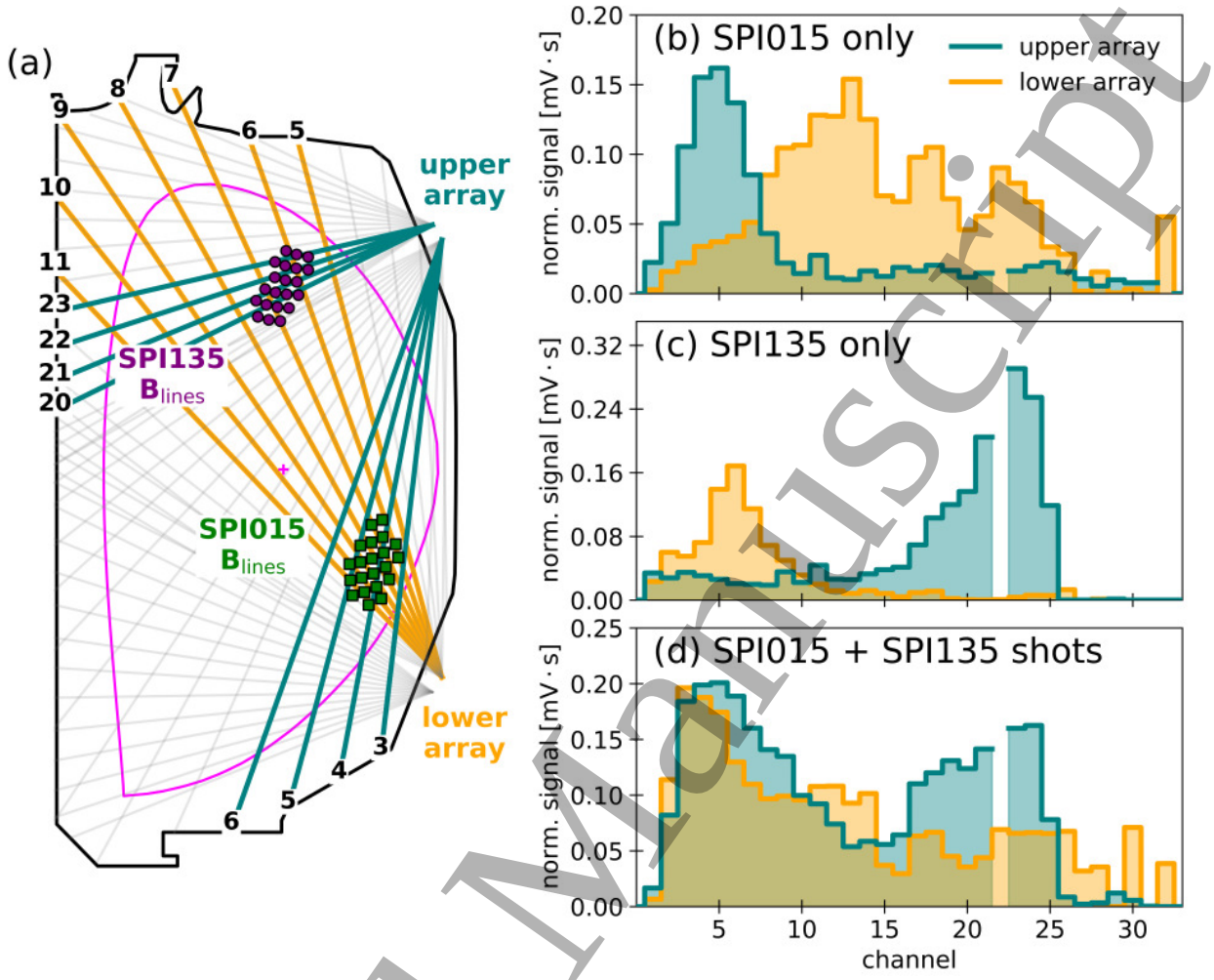

Figure 8. A cross-section of DIII-D at the location of the AXUV radiometer at 90 degrees, shown in Fig. 1 (a). Mapped field line locations at the radiometer location for SPI015 (green squares) and SPI135 (purple circles) based on the field lines at the injection location transversing a minimal toroidal distance between the injected impurities and the radiometer. Chords of the radiometer from the upper array (teal) and lower array (orange) are overlaid with specific channels intersecting the projected field lines locations highlighted. The initial TQ total integrated signal during a SPI mitigated shutdown plotted as a function of channel number for SPI015 only shots (b), SPI135 only shots (c), and the dual pellet shots coming from SPI015 and SPI135 (d).

timescales when impurities are introduced from multiple injection ports. The lower cooling duration (see Fig. 6) may limit the amount of the neon assimilated or depth of penetration by the shattered pellet into the plasma prior to the end of the TQ. One possible explanation is that these experiments injected an excessive amount of impurities compared to the energy content of the plasma. Specifically, the low Ne pellet injects additional deuterium comparable to the number of particles within the original plasma. This could result in excessive dilution cooling, limiting the amount of thermal energy required to ionize the remaining Ne. However, analysis of similar MGI experiments on DIII-D show that the cooling duration decreases for simultaneous pure Ne injections compared to single injections. Additional experiments are planned to examine dilution cooling effects.

Alternatively, the results of Section 4 suggest that the faster shutdown with two pellets could be due to the "head start" in the toroidal and poloidal spreading of impurities, compared to a single SPI, due to injecting the pellets at different toroidal locations. This essentially cools multiple flux tubes simultaneously and may induce global MHD instabilities more rapidly than a single flux tube of impurities, leading to reduced cooling duration and, subsequently, lower impurity assimilation. This raises an additional question, will the plasma cooling duration further decrease as more pellets are introduced at more than one toroidal location (or flux tube)?

Further investigation into initial radiation behavior, Fig. 8(d), shows how much the radiation from the

pure Ne injection port actually decreased. It was discussed in Section 3.4 through radiation fraction measurements that the injected impurities possibly prefer to flow in the counter-clockwise direction, towards the high-field side based on the helicity of the equilibrium field. However, why is the radiation measured from the low Ne pellet injection (near channel 5) higher in magnitude than the radiation from the pure Ne pellet (near channel 23)? Perhaps this is an artifact of the line-integrated measurement or consistent late arrival times of the pure Ne pellet within the integration window. The radiation near the low Ne injection port should increase, but is not measured due to diagnostic limitations.

Nevertheless, as evident by the reduction in global mitigation properties (such as the CQ duration), this increase is not enough to offset the decreased radiation from the pure Ne pellet, suggesting that the overall effect of the low Ne pellet is to decrease the effectiveness of the pure Ne pellet. However, simultaneous pellet injection still has better mitigation properties then when the low neon quantity pellet solely mitigates the plasma.

Additionally, increasing the background density in order to prevent runaway electrons is a current mitigation technique planned for ITER [23]. Surprisingly, despite the decreased assimilation of radiative impurities, the radial line-integrated density is observed to increase when both pellets have a simultaneous arrival and a maximum increase when both pellets arrive prior to the start of the TQ (see Fig. 7). These density measurements show that multiple pellets increase the density higher than a single pellet, but are sensitive the arrival time of the second pellet. The second pellet should arrive prior to the start of the TQ in order to effectively increase the density. This result is not unexpected, as the shattered pellet plume from the second pellet may not have the time required to penetrate deep into the plasma where the ablation and ionization rates are higher. It should be noted that depending on the SPI speed and the time required for a single SPI pellet to trigger the TQ for a larger plasma, the arrival window for the second pellet could be larger.

6. Conclusions

Experiments on DIII-D have injected multiple shattered pellets at different toroidal locations for the first time, as is planned for the ITER disruption mitigation system. Systematically varying the relative timing of the two pellets suggests that simultaneously injected pellets may impact the assimilation of each other, altering the resulting disruption characteristics compared to that due to a single pellet injecting similar neon quantities. TQ radiation measured near the injection location is reduced with the dual pellets. An increase in the measured inner strike point heat load confirms the reduced radiation fraction measurements.

The reduction in overall neon assimilation, evidenced by changes in TQ behavior, is also supported by measurements of subsequent CQ evolution. Global disruption mitigation properties are found to decrease when the pellets enter the plasma simultaneously compared to single pure Ne shattered pellet injections. The electron density increased by approximately a factor of two with the addition of multiple pellets, but is highly sensitive to the time between injections. A maximum density increase is found when both pellets arrive at the plasma prior to the start of the TQ. This density increase dropped to approximately 40% if the second pellet arrived just after the start of the TQ. The initial SPI radiation is shown to radiate along individual flux tubes along the trajectory of the shattered pellet plume. The addition of the second SPI system shows that multiple flux tubes are initially cooled simultaneously and spread out into two distinct regions.

Acknowledgments

This material is based on work supported by the U.S. Department of Energy, Office of Science, Office of Fusion Energy Sciences, using the DIII-D National Fusion Facility, a DOE Office of Science user facility, under Award Nos. DE-FC02-04ER54698, DE-AC05-00OR22725, DE-FG02-07ER54917, and DE-AC52-07N27344. DIII-D data shown in this paper can be obtained in digital format by following the links at `https://fusion.gat.com/global/D3D_DMP`.

References

[1] Hender T, Wesley J, Bialek J, Bondeson A, Boozer A, Buttery R, Garofalo A, Goodman T, Granetz R, Gribov Y, Gruber O, Gryaznevich M, Giruzzi G, Günter S, Hayashi N, Helander P, Hegna C, Howell D, Humphreys D, Huysmans G, Hyatt A, Isayama A, Jardin S, Kawano Y, Kellman A, Kessel C, Koslowski H, Haye R L, Lazzaro E, Liu Y, Lukash V, Manickam J, Medvedev S, Mertens V, Mirnov S, Nakamura Y, Navratil G, Okabayashi M, Ozeki T, Paccagnella R, Pautasso G, Porcelli F, Pustovitov V, Riccardo V, Sato M, Sauter O, Schaffer M, Shimada M, Sonato P, Strait E, Sugihara M, Takechi M, Turnbull A, Westerhof E, Whyte D, Yoshino R, Zohm H, the ITPA MHD D and Group M C T 2007 *Nuclear Fusion* **47** S128 URL http://stacks.iop.org/0029-5515/47/i=6/a=S03

[2] Commaux N, Baylor L, Jernigan T, Hollmann E, Parks P, Humphreys D, Wesley J and Yu J 2010 *Nuclear Fusion* **50** 112001 URL https://doi.org/10.1088%2F0029-5515%2F50%2F11%2F112001

[3] Commaux N, Shiraki D, Baylor L, Hollmann E, Eidietis N, Lasnier C, Moyer R, Jernigan T, Meitner S, Combs S and Foust C 2016 *Nuclear Fusion* **56** 046007 URL http://stacks.iop.org/0029-5515/56/i=4/a=046007

[4] Shiraki D, Commaux N, Baylor L R, Eidietis N W, Hollmann E M, Lasnier C J and Moyer R A 2016 *Physics of Plasmas* **23** 062516 (*Preprint* http://dx.doi.org/10.1063/1.4954389) URL http://dx.doi.org/10.1063/1.4954389

[5] Whyte D G e a 2008 Studies of requirements for iter disruption mitigation systems *Proc. 22nd Int. Conf. on Fusion Energy 2008 (Geneva, Switzerland, 2008)* (http://www-naweb.iaea.org/napc/physics/FEC/FEC2008/html/index.htm: (Vienna: IAEA) CD-ROM file IT/P6-18)

[6] Baylor L, Barbier C C, Carmichael J R, Combs S K, Ericson M N, Ezell N D B, Fisher P W, Lyttle M S, Meitner S J, Rasmussen D A, Smith S F, Wilgen J B, Maruyama S and Kiss G 2015 *Fusion Science and Technology* **68** 211–215 (*Preprint* https://doi.org/10.13182/FST14-926) URL https://doi.org/10.13182/FST14-926

[7] Combs S K, Meitner S J, Baylor L R, Caughman J B O, Commaux N, Fehling D T, Foust C R, Jernigan T C, McGill J M, Parks P B and Rasmussen D A 2010 *IEEE Transactions on Plasma Science* **38** 400–405 ISSN 0093-3813

[8] Meitner S, Baylor L R, Commaux N, Shiraki D, Combs S, Bjorholm T, Ha T and McGinnis W 2017 *Fusion Science and Technology* **72** 318–323 (*Preprint* https://doi.org/10.1080/15361055.2017.1333854) URL https://doi.org/10.1080/15361055.2017.1333854

[9] Hollmann E M, Chousal L, Fisher R K, Hernandez R, Jackson G L, Lanctot M J, Pidcoe S V, Shankara J and Taussig D A 2011 *Review of Scientific Instruments* **82** 113507 (*Preprint* http://dx.doi.org/10.1063/1.3660816) URL http://dx.doi.org/10.1063/1.3660816

[10] Gray D S, Hollmann E M, Luckhardt S C, Chalfant J, Chousal L, Hernandez R, Jones E and Kellman A G 2004 *Review of Scientific Instruments* **75** 4133–4135 (*Preprint* https://doi.org/10.1063/1.1787149) URL https://doi.org/10.1063/1.1787149

[11] Lasnier C J, Allen S L, Ellis R E, Fenstermacher M E, McLean A G, Meyer W H, Morris K, Seppala L G, Crabtree K and Zeeland M A V 2014 *Review of Scientific Instruments* **85** 11D855 (*Preprint* https://doi.org/10.1063/1.4892897) URL https://doi.org/10.1063/1.4892897

[12] Carlstrom T N, Ahlgren D R and Crosbie J 1988 *Review of Scientific Instruments* **59** 1063–1066 (*Preprint* https://doi.org/10.1063/1.1139726) URL https://doi.org/10.1063/1.1139726

[13] Moyer R A, Bykov I, Orlov D M, Evans T E, Lee J S, Teklu A M, Fenstermacher M E, Makowski M, Lasnier C J, Wang H Q, Watkins J G and Wu W 2018 *Review of Scientific Instruments* **89** 10E106 (*Preprint* https://doi.org/10.1063/1.5038350) URL https://doi.org/10.1063/1.5038350

[14] Gray D S, Luckhardt S C, Chousal L, Gunner G, Kellman A G and Whyte D G 2004 *Review of Scientific Instruments* **75** 376–381 (*Preprint* https://doi.org/10.1063/1.1642745) URL https://doi.org/10.1063/1.1642745

[15] Commaux N, Baylor L R, Jernigan T C, Hollmann E M, Humphreys D A, Wesley J C, Izzo V A, Eidietis N W, Lasnier C J, Moyer R A, Parks P B, Foust C R, Combs S and Meitner S J 2014 *Physics of Plasmas* **21** 102510 (*Preprint* http://dx.doi.org/10.1063/1.4896721) URL http://dx.doi.org/10.1063/1.4896721

[16] Lao L, Ferron J, Groebner R, Howl W, John H S, Strait E and Taylor T 1990 *Nuclear Fusion* **30** 1035 URL http://stacks.iop.org/0029-5515/30/i=6/a=006

[17] Hollmann E M, Commaux N, Eidietis N W, Lasnier C J, Moyer R A, Parks P B and Shiraki D 2015 *Physics of Plasmas* **22** 102506 (*Preprint* https://doi.org/10.1063/1.4932999) URL https://doi.org/10.1063/1.4932999

[18] ITER Physics Expert Group on Disruptions, Plasma Control, and MHD and ITER Physics Basis Editors 1999 *Nuclear Fusion* **39** 2251 URL http://stacks.iop.org/0029-5515/39/i=12/a=303

[19] Izzo V, Parks P, Eidietis N, Shiraki D, Hollmann E, Commaux N, Granetz R, Humphreys D, Lasnier C, Moyer R, Paz-Soldan C, Raman R and Strait E 2015 *Nuclear Fusion* **55** 073032 URL http://stacks.iop.org/0029-5515/55/i=7/a=073032

[20] Eidietis N W, Izzo V A, Commaux N, Hollmann E M and Shiraki D 2017 *Physics of Plasmas* **24** 102504 (*Preprint* https://doi.org/10.1063/1.5002701) URL https://doi.org/10.1063/1.5002701

[21] Evans T E, Moyer R A and Monat P 2002 *Physics of Plasmas* **9** 4957–4967 (*Preprint* https://doi.org/10.1063/1.1521125) URL https://doi.org/10.1063/1.1521125

[22] Hu D, Nardon E, Lehnen M, Huijsmans G, van Vugt D and Contributors J 2018 *Nuclear Fusion* **58** 126025 URL http://stacks.iop.org/0029-5515/58/i=12/a=126025

[23] Lehnen M, Aleynikova K, Aleynikov P, Campbell D, Drewelow P, Eidietis N, Gasparyan Y, Granetz R, Gribov Y, Hartmann N, Hollmann E, Izzo V, Jachmich S, Kim S H, Kočan M, Koslowski H, Kovalenko D, Kruezi U, Loarte A, Maruyama S, Matthews G, Parks P, Pautasso G, Pitts R, Reux C, Riccardo V, Roccella R, Snipes J, Thornton A and de Vries P 2015 *Journal of Nuclear Materials* **463** 39 – 48 ISSN 0022-3115 pLASMA-SURFACE INTERACTIONS 21 URL http://www.sciencedirect.com/science/article/pii/S0022311514007594